國立交通大學
材料科學與工程學系
碩士論文

氧對鎳誘導非晶矽結晶的影響

The Effect of Oxygen on the Ni
Induced Crystallization of Amorphous
Silicon

研究生：林佑達

指導教授：吳耀銓 博士

中華民國九十三年七月

氧對鎳誘導非晶矽結晶的影響

The Effect of Oxygen on the Ni Induced Crystallization of Amorphous Silicon

研究生：林佑達　　　　　Student　:　You-Da Lin

指導教授：吳耀銓 博士　　Advisor　: Dr. Yewchung Sermon Wu

國 立 交 通 大 學

材 料 科 學 與 工 程 學 系

碩 士 論 文

A Thesis Submitted to Department of Material Science and Engineering

College of Engineering National Chiao Tung University

In Partial Fulfillment of the Requirements for the Degree of Master of

Science in Material Science and Engineering

July 2004

Hsinchu, Taiwan, Republic of China

中 華 民 國 九 十 三 年 七 月

氧對鎳誘導非晶矽結晶的影響

研究生：林佑達　　　　　　　指導教授：吳耀銓博士

國 立 交 通 大 學

材料科學與工程研究所碩士班

摘　　要

　　本篇論文研究金屬鎳誘發非晶矽測向結晶時氧的影響。在退火過程中，使用含氧的退火氣氛並不會對金屬誘發測向結晶的長度和成長速率有影響。而鎳薄膜中若有氧的存在，也不會對其金屬誘發測向結晶的速率有所影響。然而，含氧鎳薄膜卻會阻礙多晶矽的結晶作用大約四小時。這是因為含氧鎳薄膜需要一段醞核時期，在這醞核時期中，含氧鎳薄膜還原成足夠的鎳金屬，以便於進行接下來的非晶矽結晶步驟。 除此之外，金屬鎳與非晶矽間介面若有原生氧化矽(native oxide)的殘留，則更進一步的會影響醞核時期，使之增加到六小時，並且金屬誘發測向結晶的速率也會減少到 2.2 μm/hr，而沒有原生氧化層殘留試片的結晶速率則為 4.1 μm/hr。

The Effects of Oxygen on the Ni Induced Crystallization of Amorphous Silicon

Student: YouDa Lin   Advisor: YewChung Sermon Wu

Department of Materials Science and Engineering

National Chiao Tung University
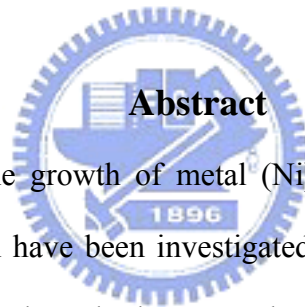
Abstract

Effects of oxygen on the growth of metal (Ni) induced lateral crystallization (MILC) of amorphous silicon have been investigated. It is found that the oxygen in the annealing ambient did not degrade the MILC length or growth rate. The oxygen existence in Ni film does not degrade the MILC growth rate either. However, it retards the nucleation of poly-Si for about 4 h. This is because that NiO_x needed an incubation period to be reduced to nickel metal for the subsequent mediated crystallization of a-Si process. In addition, the native oxide contaminated in interface between Ni and a-Si has been studied. It would impede the NiO reaction with a-Si and retards the nucleation of poly-Si for about 6 hr. The MILC rate that is 4.1 μm/hr without native oxide in interface is degraded by the native oxide for about 2.2 μm/hr in comparison.

愛你們，也以你們為榮。

僅以此篇論文獻給所有愛我關懷我的師長朋友。

Contents

Chapter 1 Introduction

Chapter 2 Experiments Items

Chapter 3 Effects of Oxygen on Metal Induced Lateral Crystallization Poly-Si Film

Chapter 4 Conclusions…………………………………………………...35

Figure Captions

Table Lists

Chapter 2

Chapter 1 Introduction

1.1 Overview of Thin Film Transistor

1.1.1 a-Si Thin Film Transistor

For the recent years, the flat panel display (FPD) has been gathered more and more attention. As the notebook, cell phone and other portable electronics are getting popular, FPD will be more important in future. There are many different kinds product of FPD, such as liquid crystal display (LCD), cathode ray tube display (CRT), plasma display panel (PDP), and organic light emitting diode (OLED). Thin film transistor liquid crystal display (TFT-LCD) was expected to become the main FPD product in portable electronics and notebook computers market. In most of TFT-LCDs, a-Si TFT played an important role to control the contrast of a pixel in TFT-LCDs. Today, TFT-LCDs gradually have become the standard component of notebook computers, desktop monitors, cell phones and other portable electronics.

In TFT-LCD process, using a-Si TFT as the pixel switching device is because of following advantages: low temperature process (< 350°C) compatible with large area glass substrate, continuous process and low leakage current property suitable for pixel switching. However, the application of a-Si TFT was constrained due to its poor field effect mobility (<1 cm^2/V·s) and small on-current. As the tendency of higher pixel density is required, the more rapid TFT will be needed. One of the solutions will be poly-Si TFT. The mobility of a-Si TFT can be improved easily by introducing poly-Si thin film instead of a-Si as an active layer of TFTs.

1.1.2 Poly-Si Thin Film Transistor

The first poly-Si TFT was proposed by Fa et at. In 1966. [1] Since then, many studies were done on the process, structure, and mechanism of poly-Si TFT to

improve the electrical performance of devices. In 1983, the first practical poly-Si TFT active matrix liquid crystal display (AMLCD) was reported. [2] Up to now, poly-Si TFTs have received lots of attention because of their wide applications in driving circuits and pixel devices of active matrix liquid crystal displays (AMLCDs) [3-7], and light emitter polymer displays (PLEDs) [8], field emission displays (FEDs) [9-11], memory devices [12-15], image sensors[16], thermal printer head[17], and photodetector amplifier[18].

For TFT-LCD applications, the poly-Si is the most promising material for obtaining high mobility TFTs. Compared with a-Si TFTs, the poly-Si TFTs have a higher carrier mobility (10~400 cm^2/V·s) [19-20], which leads to a smaller, faster device. In the LCD panel, the area of TFTs is opaque. Thus if the TFTs

1.2 Crystallization Methods for Amorphous Silicon (a-Si) Thin Film

Crystallization of a-Si thin film has been considered the most important process in the fabrication of Low Temperature Poly Si (LTPS) TFTs. The quality of crystallized poly-Si thin film strongly influences the electrical performance poly-Si TFTs because this film always play the role of active layer, or channel, in the device. In the following, three kinds of low temperature crystallization methods, which have been widely studied, are roughly reviewed, including solid phase crystallization (SPC), excimer laser crystallization (ELC), and metal induced crystallization/metal induced lateral crystallization (MIC/MILC).

1.2.1 Solid Phase Crystallization (SPC)

The simplest way for transformation a-Si to poly-Si with application to TFTs is conventional thermal annealing, called solid phase crystallization (SPC), in a conventional furnace [21-23]. However, because of the temperature limit for glass

substrate (~600°C), low temperature process must be performed. For thin film deposited at temperatures below 600°C, thermal crystallization for several hours (20~48 hours) at 600°C is required to convert them into final polycrystalline form. This phenomenon takes place because Si is imparted energy sufficient to overcome the interfacial free energy associated with the formation of critical sized crystalline nuclei and atomic mobility to the point where the transformation occurs with a reasonable rate.

The grain size of poly-Si coming from SPC is larger by several times and has smoother surface morphology than that of as-deposited poly-Si. Large defect density, nevertheless, exists in crystallized poly-Si grain as a result of the low temperature used [24]. In addition, this method is time-consuming because long crystallization durations of several hours are necessary.

1.2.2 Excimer Laser Crystallization (ELC)

Recently, excimer laser crystallization (ELC) has become a key technology to fabricate high performance poly-Si TFTs [25-26]. Excimer lasers emit in the UV region (output wavelengths 193, 248, and 308 nm for ArF, KrF, and XeCl gas mixtures, respectively) with a short pulse duration (10~30 ns). Strong optical absorption of the UV light ($\alpha > 10^6$ cm^{-1}) and small heat diffusion length during the laser pulse implies that high temperatures can be developed in the Si-surface region, causing melting, without appreciable heating (400 °C) of the substrate. This makes the ELC process compatible with glass substrates and even plastics, one of the major advantages of this technique. Another advantage is that the poly-Si obtained has a good crystallinity with very few in-grain defects, due to the melt-regrowth process. Depending upon the laser energy density, crystallization mechanism can be divided into three transformation regimes [27-28]. Those are the low and high energy density

regimes, and the so-called super lateral growth (SLG) regime between them.

Low energy density regime (partial melting regime)

The low energy density regime indicates the situation that the energy density of incident laser pulse is larger than the threshold energy of crystallization but is still low so that only partial a-Si area on the top would be melted and leave a continuous layer of solid Si remains (i.e. melt-depth < film thickness). Therefore, this energy range is also referred to as partial melting regime. The poly-Si grains would grow from bottom to top and the lateral growth would be confined by each other, and the grain size increases with energy density.

High energy density regime (complete melting regime)

In the high energy density regime the incident energy density is high enough to melt the a-Si film entirely. It is also called as the complete melting regime. Small-grained poly-Si is formed because of the homogeneous nucleation coming from a deep supercooling of the melt [29].

Super lateral growth regime (near complete melting regime)

At the transition between the two major regimes described above, crystallization leads to formation of large-grained poly-Si grained poly-Si with grain sizes many times larger than the film thickness [27-28, 30]. It is suggested that at the maximum point of melting the unmelted portion of the underlying Si on longer forms a continuous layer but instead consists of islands of solid that are separated by small local regions of completely melten silicon. The un-melted islands act as solidification seeds, from which a lateral grain growth commences. This energy range is also referred to as the near complete melting regime. The resulting grain size can exceed

the film thickness by up to a factor of 20 to 30.

1.2.3 Metal Induced Crystallization (MIC) and Metal Induced Lateral Crystallization (MILC)

Even though SPC is a low-cost process, the normal crystallization temperature of a-Si is still too high for the glass substrate, taking excessive annealing duration. It is well known that SPC temperature of a-Si can be lowered by the addition of certain metals. Such behavior is called metal induced crystallization (MIC). Among various metals, they can be classified into two groups. One is eutectic-forming metals such as Ag [31], Au [32], Al [33], Sb [34], and In [35]; the other is silicide-forming metals including Pd [36-37], Ti [38], Ni [39], and Cu [40]. The former are to increase Si atomic mobility by forming interstitials which change the Si-Si bonding nature from covalent to metallic [41-42], or to form low temperature eutectic [43] or metal stable silicide compounds [32] which undergo crystallization at lower temperature than pure a-Si. The latter are thought to form a crystalline metal silicide, which acts as a heterogeneous nucleation site for Si crystallization. Although the crystallization temperature is reduced significantly, metal contamination is a serious problem in MIC poly-Si film. Nickel (Ni) was found to induce crystallization of a-Si outside its coverage area [44-45]. This phenomenon referring to as metal induced lateral crystallization (MILC) has been found to produce polycrystalline silicon thin film largely free of metal contamination, with better crystallinity than those produced by SPC. The mechanism of Ni silicide mediated crystallization is introduced as follow.

In the initial stage, the nucleation of c-Si occurs randomly at the {111} faces of an individual octahedral $NiSi_2$ precipitate [46]. The orientation of the $NiSi_2$ precipitates within the a-Si determines both the orientation of initial crystalline structure and the subsequent growth direction of needlelike crystallites. All kinds of

crystallites grow in the <111> direction, which is normal to $NiSi_2$ {111} planes. The growth of {111} faces can be explained by the fact that the surface free energy of the {111} plane in Si is lower than that of any other orientation. Also, the small lattice mismatch (0.4%) between $NiSi_2$ and Si facilitates the formation of epitaxial c-Si on the {111} faces of the $NiSi_2$ precipitates. Following nucleation of crystallites on the $NiSi_2$ precipitates, needlelike c-Si grows at the $NiSi_2$/c-Si interface as the $NiSi_2$ precipitates migrate through the a-Si.

1.3 Motivation

Compare with ELC, the disadvantage of MILC is a long time process; however, the advantage of MILC is low cost. So many scientists were engaged in increasing the MILC rate such as FALC or higher annealing temperature process, but these methods are going to raise the cost of MILC process.

So this paper focuses on reducing the cost of MILC method. The Ni film was usually deposited on a-Si film by PVD method in MILC process. From previous studied, the requirement of purity of Ni must be 99.999%, so the Ni must be deposited under ultra high vacuum (UHV) condition. The UHV process and apparatuses are an time-consuming and a high cost process. To reducing the cost, an alternative Ni deposition process, Ni depositing in low vacuum about 75 torrs, was used, and the affection of oxygen in Ni film during MILC process was investigated.

Furthermore, taking annealing ambient into consideration, literature reviews showing the protective ambient, such as N_2 or Ar ambient, was needed. The degree of how would oxygen ambient affect the MILC rate was studied.

In sum, the experiment described in this work was performed to investigate the effect of oxygen on Ni induced crystallization of a-Si and to determine the necessity of the nitrogen ambient and UHV deposition system for crystallization of a-Si.

Chapter 2 Experimental Items

The complete description of experimental items would be given in this chapter. In the first section, an overview of the experimental procedure is shown, and each experimental step is dilated on the remaining sections.

2.1 Experimental Procedure

The directions of this work which can be partitioned into three parts are shown in Fig. 2-1:

- Ambient effect in MILC process

  - The effect of a-Si thickness

  - The effect of the oxide/Si interface

- Oxygen concentration in Ni film

- Oxygen contamination at Ni/a-Si interface

The detail information of the preparation of samples is illustrated in section below.

2.1.1 The Preparation of a-Si Thin Film

Silicon (100) wafers were used as the substrates in this study. Wet oxide film of 500 nm thickness were grown by using a H2/O2 mixture at a substrate temperature of 1050℃. Silane-based a-Si film with a thickness of 100 nm were then deposited by a low-pressure chemical vapor deposition (LPCVD) system at 550℃.

2.1.2 The Deposition Processes of Ni and NiO$_x$ Films

Four kinds of samples were used in this work. Their specifications are listed in Table I. Nickel or nickel oxide films were deposited on the top of a-Si. They were

designated as "Ni" and "NiO", respectively. Prior to loading the wafers into the deposition chamber, the native silicon oxide on the a-Si film was removed by dipping the wafers in diluted HF. The Ni film was deposited by DC sputter at room temperature. The base pressure in the deposition chamber was 10-6 torr, but rose to 8 x10-3 torr during the deposition. The total thickness deposited was about 10 nm. As for the NiO film, it was deposited by a cold DC sputter in air atmosphere [52]. The thickness was also about 10 nm. A lift-off process using photoresist was employed to form islands of Ni or NiO on the wafers. The photoresist was first patterned to expose selected regions of the a-Si thin film. After the deposition of the metal film, the wafers were dipped in acetone to dissolve the photoresist and to lift off unwanted metal.

2.1.3 Metal Induced Lateral Crystallization Process

A schematic illustration shown in Fig. 2-2 displays the process procedure of metal induced lateral crystallization (MILC) in which Ni is utilized as metal material. After a-Si deposited on the wet-oxide silicon wafer successfully, photoresist was spin on the a-Si surface and then a seed window was developed by photolithography technique to prevent a-Si outside the seed window from contacting with Ni. Subsequently, metal induced crystallization (MIC) and MILC were carried out by thermal annealing at the temperature of 500℃ or above for various annealing time.

2.1.4 The Annealing Condition of MILC Process

Wafers were then cut into 1x 1 cm^2 samples for the subsequent heat treatment. The heat treatment was carried out at 550℃ for 1 to 24 h. Wafers were then annealed either in nitrogen or oxygen atmosphere. They were labeled as "Ni-N", "NiO-N", "Ni-O" and "NiO-O", respectively, shown in Table 1.

2.2 Material Characterization of Metal Induced Lateral Crystallization

An optical microscope (OM) was used to measure the MILC length. A scanning electron microscope (SEM) was employed to observe the morphology of the MILC region and a transmission electron microscope (TEM) was analyzed and define the grain structure of MILC poly Si.
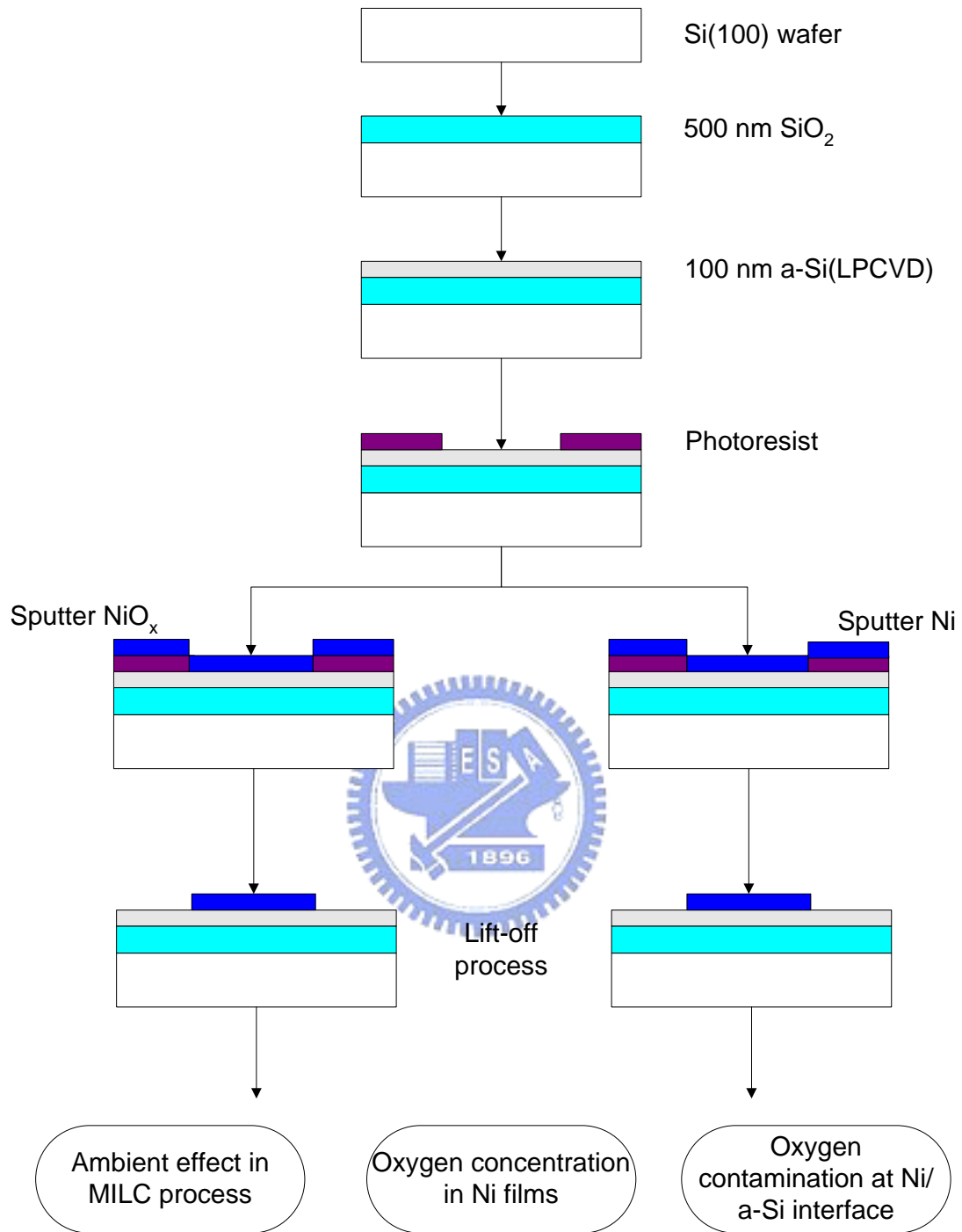
Fig. 2-1: The directions of this work and the process of experiment are shown.

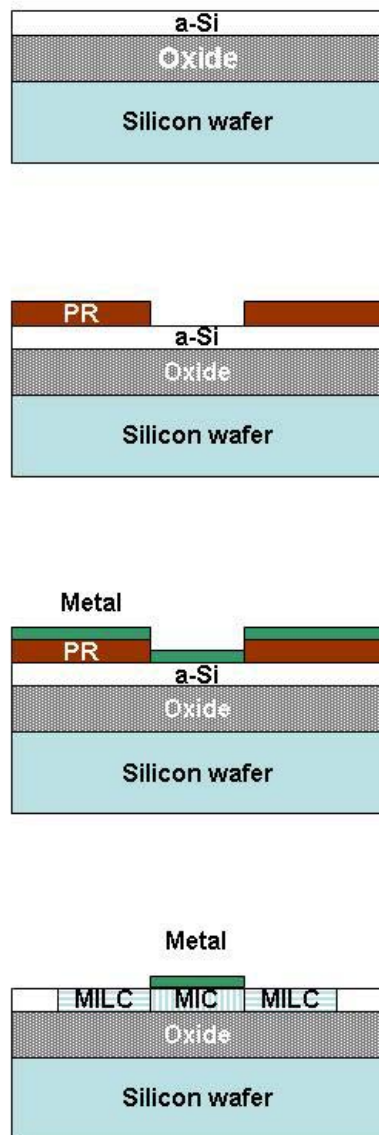Fig. 2-2: Schematic illustration of MILC process

Table 2-1: Summary of sample preparation parameters

	Ni-N	Ni-O	NiO-Ni	NiO-O
Deposition metal	Ni	Ni	NiO	NiO
Annealing ambient	Nitrogen	Oxygen	Nitrogen	Oxygen

Chapter 3 Effects of Oxygen on Metal Induced Lateral Crystallization Poly-Si Film

This chapter discusses the oxygen effect in MILC process. There are three possible aspects. The first is the annealing ambient during MILC process. The second is oxygen concentration in the Ni film. The third is the oxygen contamination between Ni and a-Si film interface.

Figure 3-1 shows the MILC induced by Ni lines with width of 300 μm. The light region at the periphery of the metal islands was the poly-Si area, which was composed of needlelike Si grains. As shown in Fig. 3-2, the diameter of needlelike grains was about 50 nm. SEM was also used to study the morphology of the MILC region. A typical SEM image of the poly-Si film after being dipped in the Secco solution [51] was shown in Fig. 3-3. The morphologies of NiO-N, Ni-O and NiO-O samples were similar to that of Ni-N set. The only difference was that the MILC lengths of Ni-N and Ni-O sets were longer than those of NiO-N and NiO-O sets.

3.1 The effect of oxygen in the annealing ambient

The MILC length perpendicular to the edge of the metal islands is plotted as a function of the annealing time in Fig. 3-4. The MILC rate as a function of the annealing time has been estimated by the slope of the curve in Fig. 3-4, and plotted in Fig. 3-5. It can be seen that the MILC length of Ni-N set was the same as that of Ni-O set, while that of NiO-N set was the same as that of NiO-O set. In other words, when samples were annealed at 550 ℃, the oxygen ambient did not degrade the MILC

growth rate.

TEM analysis revealed that an oxide layer was formed on the top of Si film. Its thickness was about 2 nm, which was similar to the value, 2 nm, simulated by SUPREM-IV program. The formation of this oxide layer will (1) decrease Si thickness and (2) create an oxide/Si interface on the top of Si. However, these two changes did not affect the growth rate of MILC. The detailed analysis is discussed in the following section.

3.1.1 The effect of the Si thickness

The effect of the a-Si thickness on the MILC Si has been reported by Ma and Wong [46] who induced crystallization of a-Si film with different thickness. After the samples were annealed at 550 ℃ for 24 h, they found that the MILC length (growth rate) decreased very slowly with decreasing thickness from 100 to 30 nm, shown in Fig. 3-6. In our study, with the formation of the oxide layer, the change of a-Si thickness was about 2 nm. The growth rate only changed a little. Therefore, the difference of the MILC lengths was too little to be measured.

3.1.2 The effect of the oxide/Si interface

The effect of the oxide/Si on the growth of MILC Si has been reported by Jin et al [52]. In their Ni induced crystallization of a-Si studies, two kinds of a-Si films were used: (1) 100 nm a-Si film and (2) 100 nm a-Si film capped by 100 nm of low temperature oxide (LTO), shown in Fig. 3-7. After the samples were annealed at 500 ℃ for 70 h, they found that the MILC lengths of these two sets of samples were the same, meaning that the oxide/Si interface had no effect on the MILC growth rate.

Since neither Si thickness nor oxide/Si interface will degrade the MILC growth rate, the oxygen in the annealing ambient will not degrade the MILC growth rate.

## 3.2 The effect of the oxygen concentration in the Ni films

The lengths of MILC changed with time at various annealing temperatures were shown in Fig. 3-8, Fig. 3-4, and Fig. 3-9, respectively. In Fig. 3-8, the NiO set didn't show the MILC phenomena at 500℃, but the Ni set did. In Fig. 3-4 and Fig. 3-9, NiO sets were shown the same slope with Ni sets at 550℃ and 600℃, respectively. It meant the Ni and NiO sets had the same MILC rate to induce a-Si crystallization.

The oxygen existence in the Ni film deteriorates the growth of MILC Si, as shown in Fig. 3-4 and 3-5. The MILC lengths of Ni-N and Ni-O sets were always higher than those of NiO-N and NiO-O sets. Surprisingly, all of their growth rates (~4.1μm/h) remained the same, regardless of the oxygen concentration in Ni. The only difference was that NiO-N and NiO-O sets needed a 4 h incubation period to start the crystallization of a-Si, but Ni set did not. In other words, the oxygen in the Ni film retarded the "nucleation" of poly-Si, but had little effect on the "growth rate" of poly-Si.

This phenomenon happened because that, in the Ni–silicide mediated crystallization of a-Si [53], the silicide precipitates acted as nucleation sites and crystallization of silicon proceeded via the migration of the precipitates through the a-Si. It required Ni to react with Si to form silicide as a nucleation site. Therefore, in the NiO set, NiO first needed to be reduced to nickel metal for the subsequent

crystallization process. From this perspective, the reaction between nickel oxide and silicon is written as follows:

$$2NiO_{(s)} + Si_{(s)} = SiO_{2(s)} + 2Ni_{(s)}$$
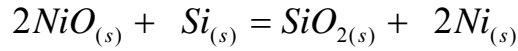
The reaction should be favorable if the change of the Gibbs free energy, ΔG^0, is negative. This free energy is equal to the formation free energy of the product of the reaction minus that of the reactant. For the reaction $Si_{(s)} + O_{2(g)} \rightarrow SiO_{2(s)}$, the formation (standard) free energy[54]

$$\Delta G^0_{SiO_2} = \text{-907,000+175T} \quad joules$$

As for the reaction $2Ni_{(s)} + O_{2(g)} = 2NiO_{(s)}$,
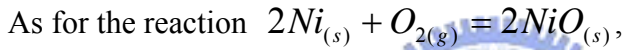
$$\Delta G^0_{NiO} = \text{-471,200+172T} \quad joules$$

Thus the change of the Gibbs free energy of the reaction

$$2NiO_{(s)} + Si_{(s)} = SiO_{2(s)} + 2Ni_{(s)},$$
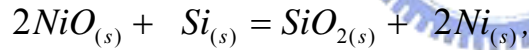
$$\Delta G^0 = \Delta G^0_{SiO_2} - \Delta G^0_{NiO} = \text{-435,900+3T} \quad joules$$

At 550 ℃, the change of the Gibbs free energy

$$\Delta G^0_{550^o C} = \text{-433,431 joules}$$

Since the Gibbs free energy for the reaction is negative, NiO could be reduced to nickel metal for the subsequent crystallization process. However, the whole crystallization process was retarded for about 4 h due to the accumulation of enough Ni metal for the subsequent mediated crystallization process.

After the 4 hour incubation period, the growth rate of NiO system was the same as that of Ni. This is because that, in the MILC process, only 5 Å thick Ni in contact

with Si was needed for the subsequent crystallization process [49]. Since the reaction byproduct, SiO2, was left behind the Ni (silicide), it had no effect on the subsequent growth rate.

Another evidence for MILC of NiO system is below. We took two NiO samples; two samples were annealed at 550℃ for 6 and 9 hours, respectively. According to the Fig. 3-4, MILC phenomena could have been observed on these two samples. After 550℃ annealing, the post annealing at 500℃, 12 hour was followed by annealing at 550℃, 6 and 9 hours, respectively. The increase of MILC length was noticed. It might be because of the MILC front, where contained $NiSi_2$, still migrating to a-Si region at 500℃. Thus, the NiO sets overcame the barrier of MILC and accumulate enough Ni to form $NiSi_2$ at 550℃, so that the MILC length would still increase in post annealing at 500℃.
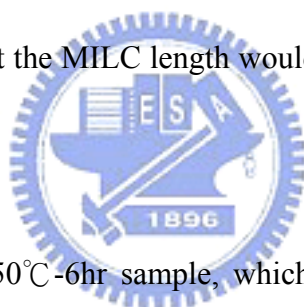
Moreover, the rate of 550℃-6hr sample, which was followed by 500℃-12hr, was different with that of 550℃-9hr sample, followed by 500℃-12hr. These phenomena illustrated in Fig. 3-10 shows that the rate of 550℃-6hr sample was lager than that of 550℃-9hr. However, the data shown in Fig. 3-11 were another sample, which was annealing in 550℃ for 169 hour. At the beginning of the annealing, the slope, the rate of MILC, was maintained in a constant value which is about 3.9 μm/hr, but as long as the sample annealed after 72 hours was shown the saturation of the MILC rate. From the SEM image of annealed secco-etch sample shown in Fig. 3-12, 550℃-24hr sample was shown more the SPC poly Si than 550℃-12hr sample. This SPC poly Si would restrain the growth of MILC in a-Si film, because the Ni silicide could not continue to transform poly Si when the sicilide of the MILC front met the SPC poly Si, shown in Fig. 3-12. In addition, the driving force between a-Si and

MILC poly Si is bigger than that between SPC poly Si and MILC poly Si. Thus, the more annealing time was used, the slower MILC rate would be. These phenomena can explain that the smaller rate of 550℃-9hr sample than 550℃-6hr sample in the same annealing condition, which is annealed in 500℃-12hr.

3.3 The Oxygen Contamination at Ni/ a-Si interface

The oxygen contamination at the a-Si surface would form native oxide. This section will discuss how the native oxide affects the growth of MILC. The experiment was used below, also shown in Fig. 3-13. The two sets of prepared a-Si sample, one was dipped in HF solution before Ni deposited, and the other was not. The sample without HF dipped would have a thin native oxide between NiO_x and a-Si interface. Two samples were gone into annealing, and the figure of the MILC length versus the annealing time was shown in Fig. 3-14. In Fig. 3-14, the length of MILC was a function of annealing time, and the rate of MILC could be estimated by the slope of the curve in Fig. 3-14. The MILC rate of NiO without HF dipped sets (NiO w/o HF sets) had been degraded more serious than NiO with HF dipped sets (NiO w HF sets), and the nucleation time of NiO w/o HF sets had been retarded by 6.1 hours.

One of the reasons which we suggest is illustrated in Fig. 3-15. The porous native oxide would form on the a-Si surface in NiO w/o HF sets, and it would prevent the reaction between NiO and a-Si by the separation of contact area within the interface between NiO and a-Si. The nucleation time would be extended, because there were not enough Ni which was produced from the reaction of NiO and a-Si to form nucleation sites of poly Si in first 6.1 hours. In addition, the native oxide would block Ni reacting with a-Si layer to form the silicide, so that the MILC rate of the NiO

w/o HF sets were less than that of the NiO w HF sets.

It would take longer time in nucleation of poly Si and smaller rate in MILC that oxygen contaminated in Ni/a-Si interface. The MILC rate of the NiO w/o HF was slowed down to 2.23 μm/hr, and the nucleation time of poly Si was elongated to 6.1 hours.
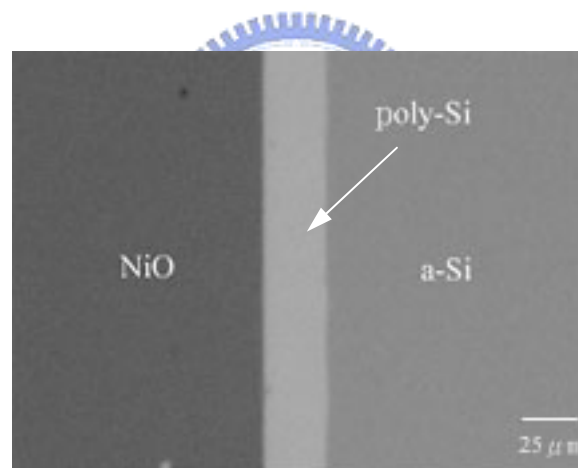
(a)
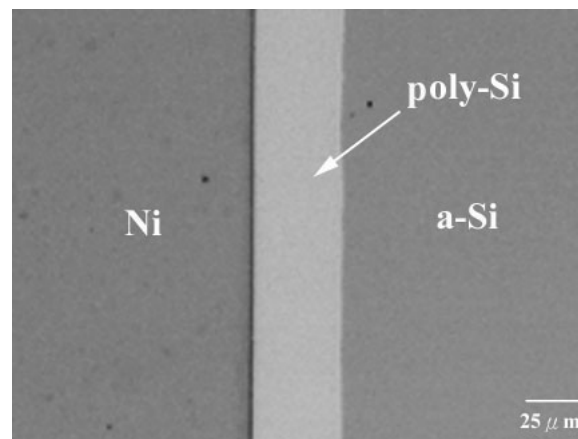
(b)

Fig. 3-1: These two images were observed by OM. MILC was induced by metal line with width of 300 μm for 550℃, 12 hours. The light region is poly Si area which is consisted of needle-like Si grain.
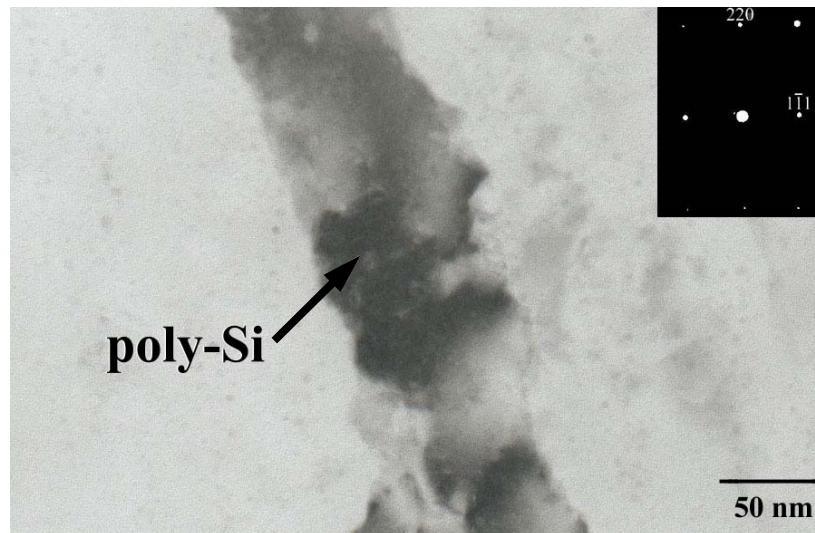
Fig. 3-2: The needle-like grain of MILC region was shown in TEM analysis. The width of the poly Si is 50 nm. The insert photography on the right-up corner is the diffraction pattern from needle-like poly Si.
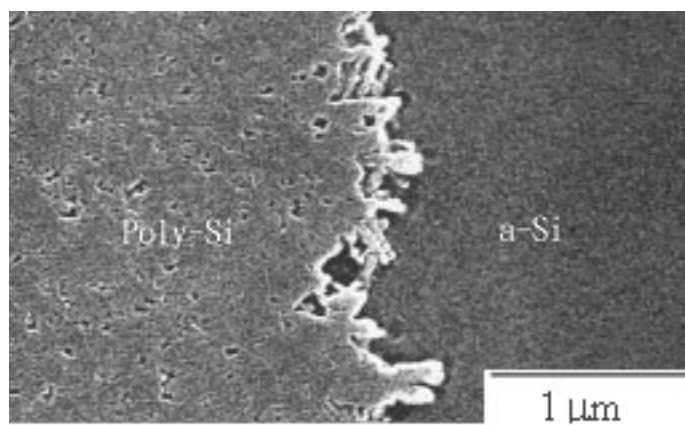
(a) Ni sets
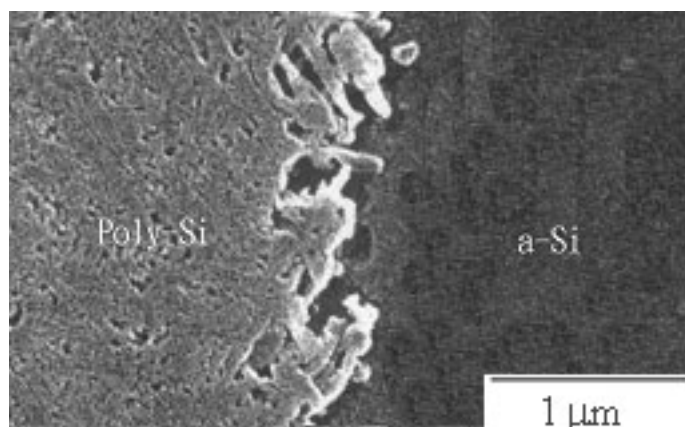
(b) NiO sets

Fig. 3-3: SEM image of Secco-etched Ni-N sample annealed at 550 °C for 12 hours.
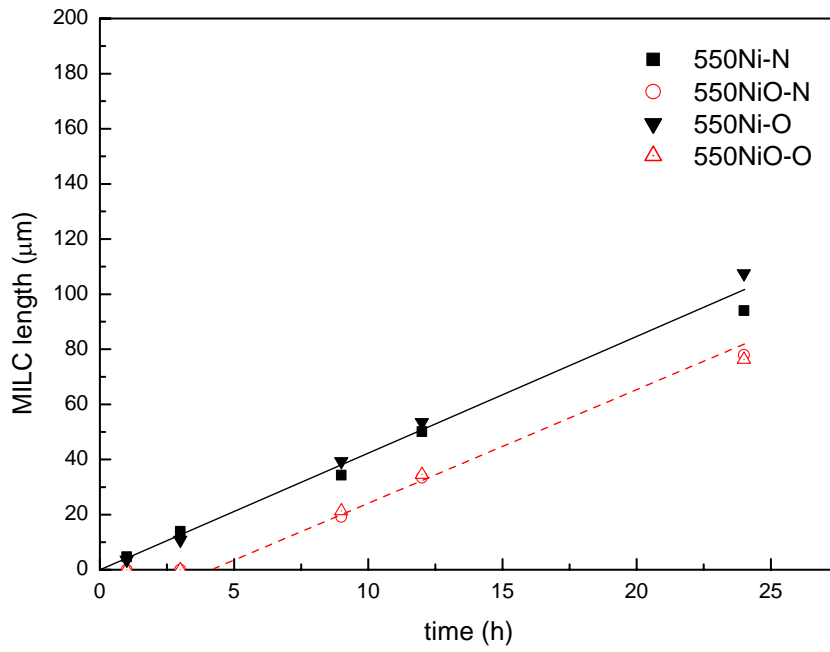
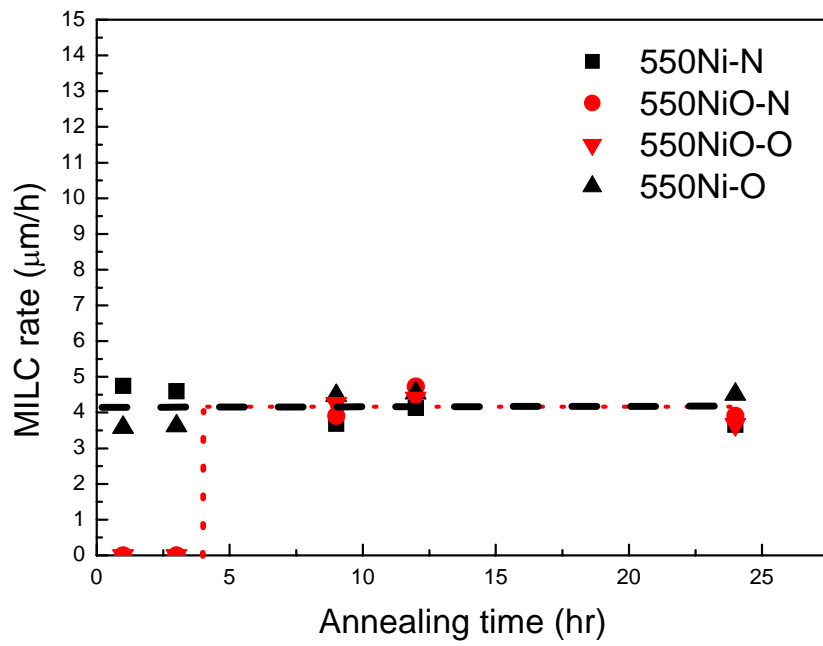Fig. 3-4: The MILC length as a function of the heat treatment time at 550 ℃

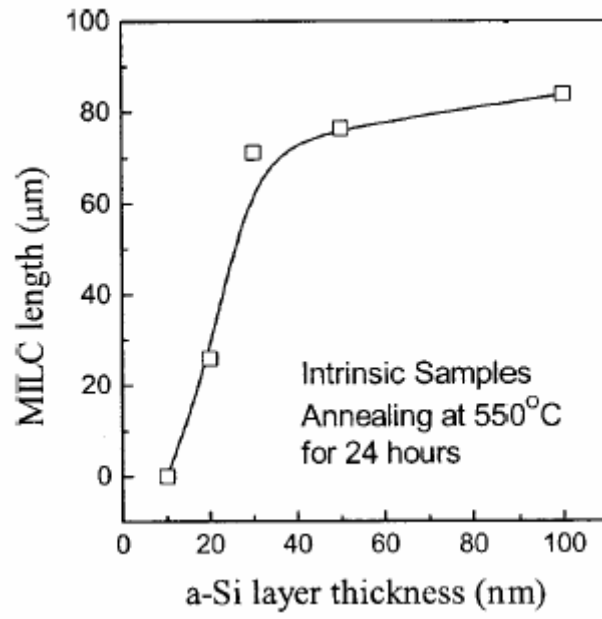Fig. 3-5: The dependence of the MILC rate on the annealing time

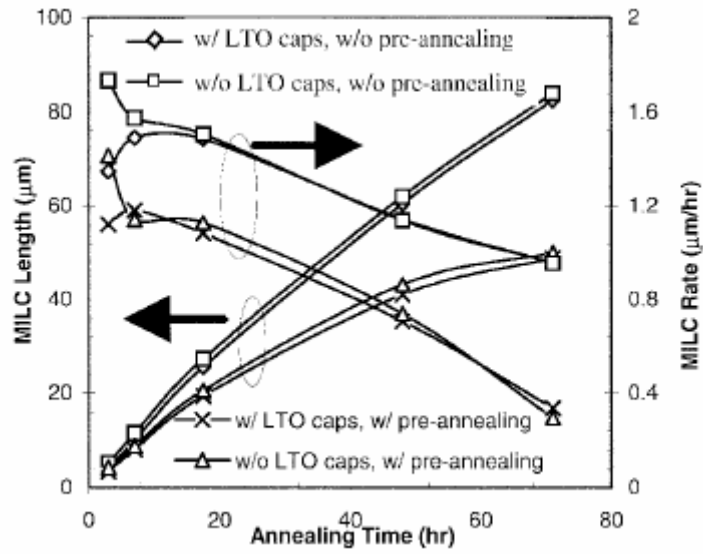Fig. 3-6: The dependence of MILC length on *a*-Si layer thickness after heat treatment at 550 °C for 24 h.

Fig. 3-7: The dependence of the MILC length and rate on the heat treatment time, with or without the pre-annealing.
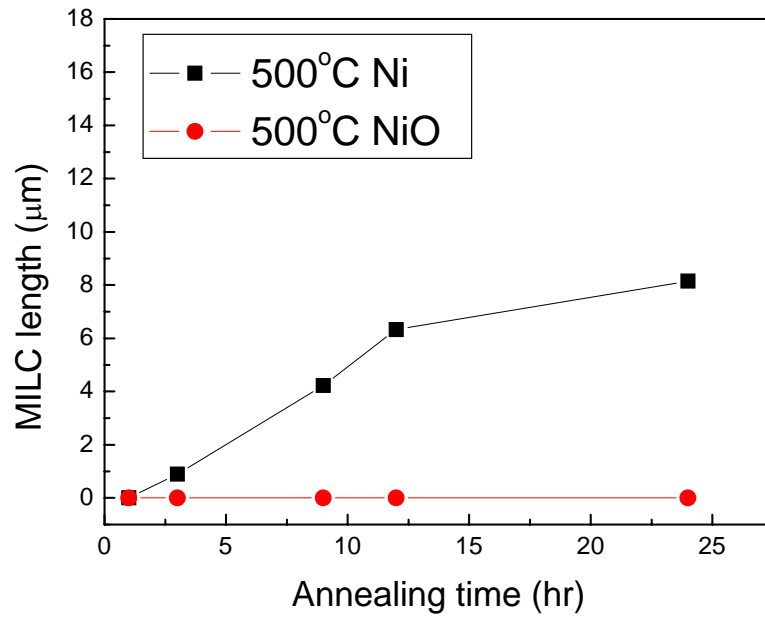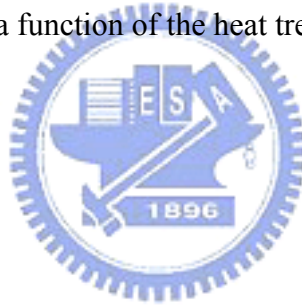
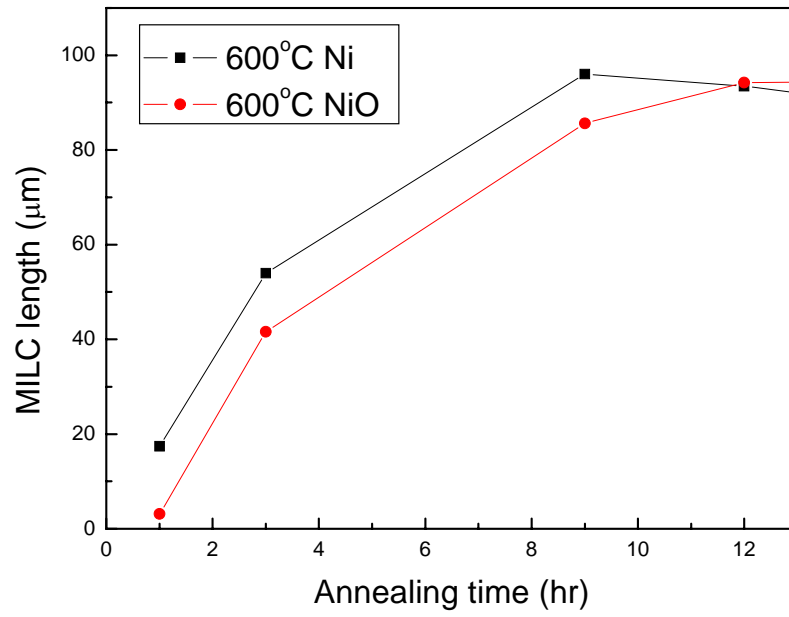Fig. 3-8: The MILC length as a function of the heat treatment time at 500 ℃

Fig. 3-9: The MILC length as a function of the heat treatment time at 600 ℃
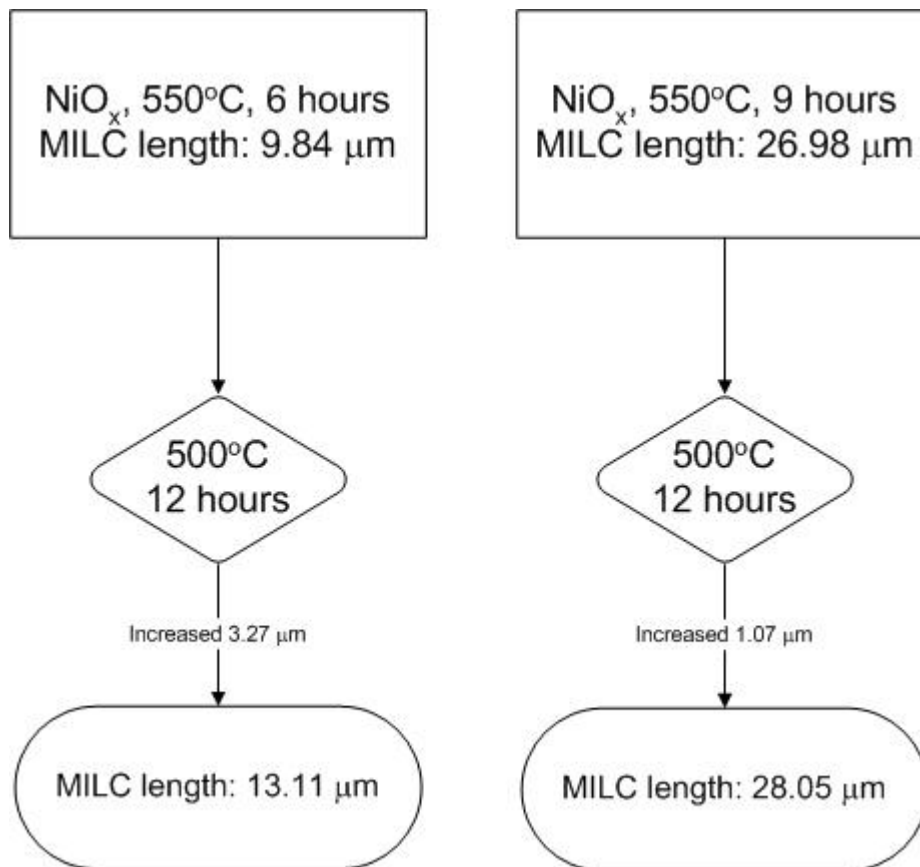
Fig. 3-10: The difference of MILC length between 550℃-6hr sample and 550℃-9hr sample after annealing in the same temperature are illustrated.
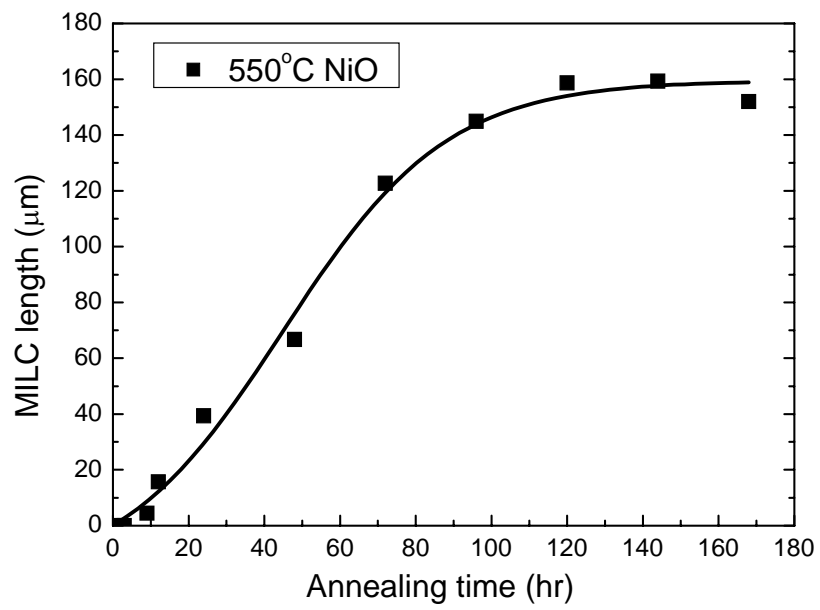
Fig 3-11: the NiO-N sample annealed in 550℃ for 168 hour.
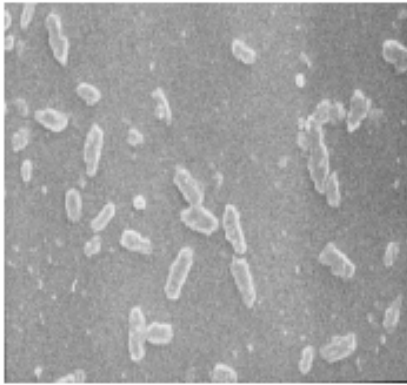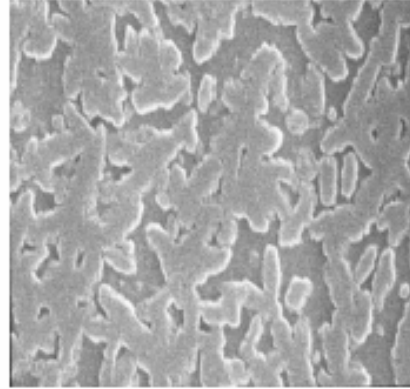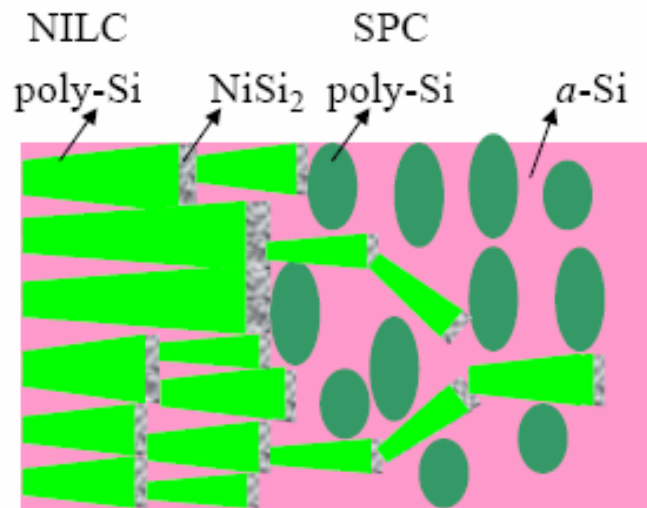
Fig 3-12: the SEM image of a-Si film annealed in 12 hour and 24 hour after secco-etching were shown. And the front of MILC poly Si retarded by SPC poly Si was illustrated.
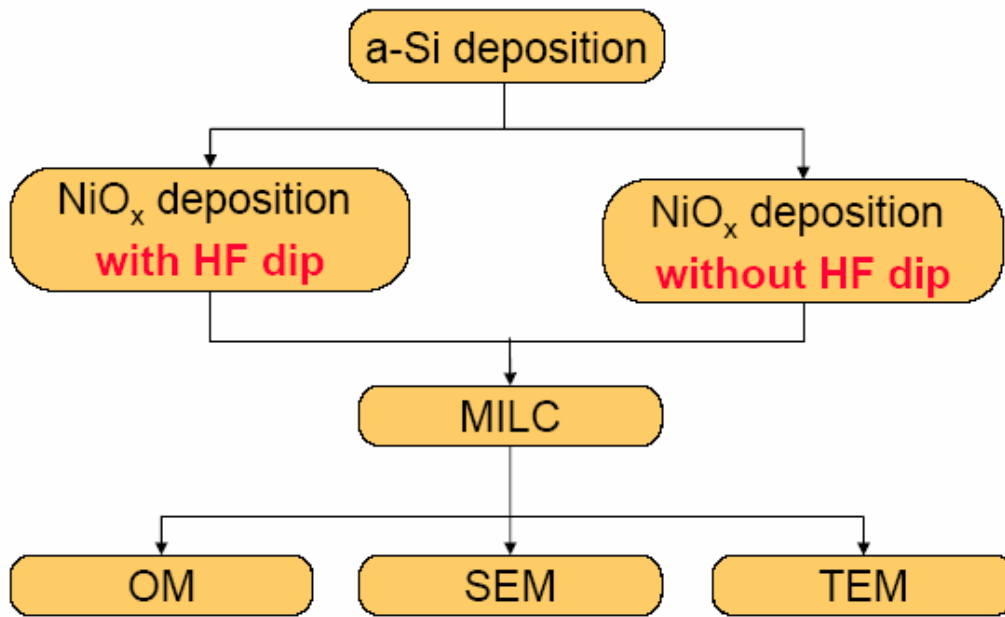
Fig. 3-13: The experiment flow chart for native oxide effect in MILC.

Fig. 3-14: The effect of native oxide in MILC length which was as a function of the heat treatment time at 550℃

Fig. 3-15: The model for effect porous native oxide in MILC procedure.

Chapter 4 Conclusion

From study mentioned before, no MILC was observed at 500℃ in NiO$_x$ sets, but at 550℃ and 600℃, the MILC of NiO sets were occurred. Because of overcoming the barrier of MILC and accumulating enough Ni of the NiO sets were to form NiSi$_2$ at 550℃ and above, so that the MILC length would still increase in post annealing at 500℃.

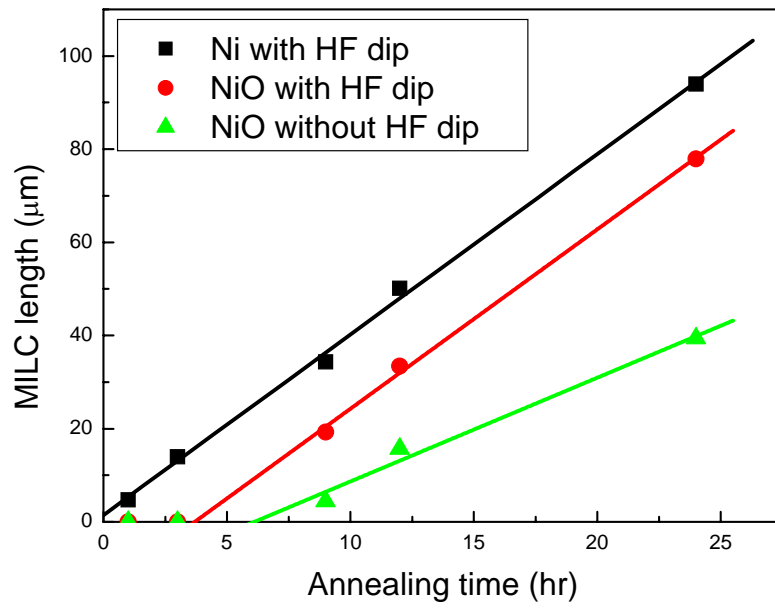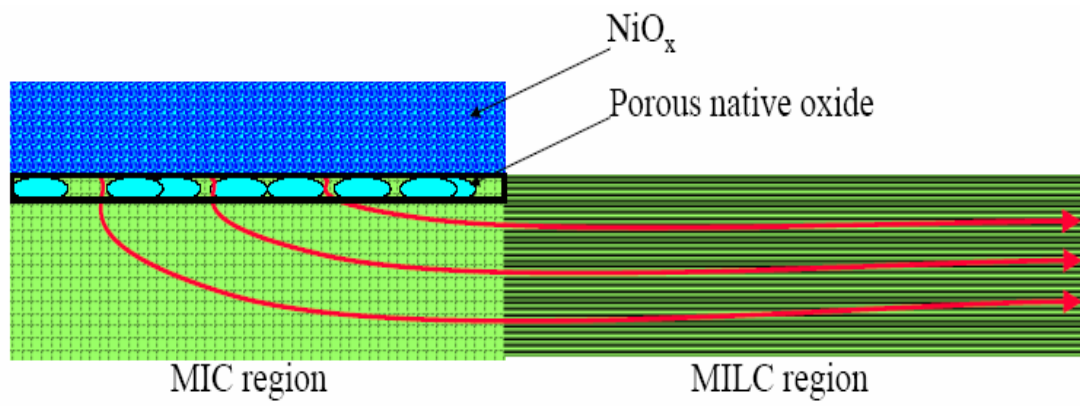Two kinds of annealing ambients (nitrogen and oxygen) and two kinds of metal films (Ni and NiO) were used to study the effects of oxygen on Ni induced crystallization of a-Si. From the aspects, the reduction of a-Si thickness and the interface between oxide and a-Si, it was found that the oxygen ambient did not degrade the MILC length or growth rate. In other words, nitrogen ambient is not a crucial part in crystallization of a-Si.

On the other hand, the oxygen concentration in Ni film did not degrade the MILC growth rate, either. However, it retarded the nucleation of poly-Si for about 4 h. This is because that NiO needed an incubation period to be reduced to nickel metal for the subsequent mediated crystallization of a-Si process.

In the sides of oxygen contamination between Ni and a-Si interface, experimental results shown that incubation time of the NiO w/o HF sets was longer than that of the NiO w HF sets and the rate of MILC in NiO w/o HF sets was smaller than that in NiO w HF sets. The MILC rate of the NiO w/o HF was slowed down to 2.23 μm/hr, and the nucleation time of poly Si was elongated to 6.1 hours.

Reference:

1. C. H. Fa and T. T. Jew, IEEE Trans. On Electron Devices, vol. 13, p. 290(1966)

2. S. Morozumi, K. Oguchi, S. Yazawa, T. Kodaira, T. Kodaira, H. Ohshima, and T. Mano, SID Dig., p. 156 (1983)

3. Y. Aoki, T. Iizuka, M. Karube, T. Tsunashima, S. Ishizawa, K. Ando, H. Skurai, T. Ejiri, T. Nakzono, M. Kobayashi, H. Sato, N. Ibaraki, M. Sasaki, N. Harada, SID 99 Dig., p. 176 (1999)

4. Mimura, N. Knishi, K. Ono, J-I Ohwada, Y. Hosokawa, Y. A. Ono,   Y. Suzuki, K. Miyata, and H. Kawakami, IEEE Trans. Elec. Dev., vol. 36, p. 351 (1989)

5. G. Lewis, D. D. Lee, and R. H. Bruce, IEEE J. Solid-State Circuits, vol. 27, p. 1833 (1992)

6. G. Lewis, I-W Wu, T. Y. Huang, A. Chiang, and R. H. Bruce, IEDM 90, p. 843, (1990)

7. T. Marita, Y. Yamamoto, M. Itoh, H. Yoneda, Y. Yamane, S. Tsuchimoto, F. Funa, and K. Awane, IEDM Tech. Dig., p. 841 (1995)

8. Simon W-B. Tam, Y. Matsueda, H. Maeda, M. Kimura, T. Shimoda and P. Migliorato, IDW '99, Sendai Int. Center, Sendai, Japan (1999)

9. H. Gamo, S. Kanemaru, and J. Itoh, Appl. Phys. Lett. Vol. 73, p. 1201 (1998)

10. H. Gamo, S. Kanemaru, and J. Itoh, Jpn. Appl. Phys. Vol. 37, p. 7134 (1998)

11. H. C. Cheng, W. K. Hong, F. G. Tarntair, K. J. Chen, J. B. Lin, K. H. Chen and L. C. Chen, Electrochem. Solid-State Lett., vol. 4, P. H5 (2001)

12. S. d. S. Malhi, H. Shichijo, S. K. Banerjee, R. Sundaresan, M. Elahy, G. P. Polack, W. F. Richardson, A. H. Shah, L. R. Hite, R. H. Womack, P. K. Chatterjee, and H. W. Lam, IEEE Trans. Elec. Dev., vol. 32, p. 258 (1985)

13. T. Yamanaka, T. Hashimoto, N. Hasegawa, T. Tanaka, N. Hashimoto, A. Shimizu, N. Ohki, K. Ishibashi, K. Sasaki, T. Nishida, T. Mine, E. Takada, and T. Nagano,

IEEE Trans. Elec. Dev., vol. 42, p. 1305 (1995)

14. K. Yoshizaki, H. Takahashi, Y. Kamigaki, T. Yasui, K. Komori, and H. Katto, ISSCC Digest of Tech. Papers, p. 166 (1985)

15. N. D. Young, G. Harkin, R. M. Bunn, D. J. Mcculloch, and I. D. French, IEEE Trans. Elec. Dev., vol. 43, p. 1930 (1996)

16. T. Kaneko, Y. Hosokawa, M. Tadauchi, Y. Kita, and H. Andoh, IEEE Trans, Elec. Dev., vol. 38, p. 1086 (1991)

17. Y. Hayashi, H. Hayashi, M. Negishi, T. Matsushita, IEEE Solid State Circuit Conference (ISSCC), p. 266 (1998)

18. N. Yamauchi, Y. Inaba, and M. Okamura, IEEE Photonic Tech. Lett., vol. 5, p. 319 (1993)

19. S. K. Kim, K. C. Park and J. Jang, J. Appl. Phys., vol. 77, p. 5115 (1995)

20. R. Dassow, J. R. Kohler, Y. Helen, K. Mourgues, O. Bannaund, T. Mohammed-Grahim, J. H. Werner, Semicond. Sci. Technol., vol. 15, p. L31 (2000)

21. M. K. Hatalis, and D. W. Greve, IEEE Elec. Dev. Lett., vol. 8, p. 361 (1987)

22. T. Aoyama, G. Kawachi, N. Konishi, T. Suzuki. Y. Olajima, and K. Miyata, J. Electrochem. Soc., vol. 136, p. 1168 (1989)

23. T. W. Little, K. Takahara, H. Koike, T. Nakazawa, I. Yudasaka, and H. Ohshima, Jpn. J. Appl. Phys., Part 1, vol. 30, p. 1789 (1991)

24. M. Bonnel, N. Duhamel, L. Haji, B. Loisel, and J. Stoemenos, IEEE Elec. Dev. Lett., vol. 14, p. 551 (1993)

25. T. Sameshima, M. Hara, and S. Usui, Jpn. J. Appl. Phys., Part 1, vol. 28, p. 1789 (1989)

26. H. Kuriyama et al., J. Appl. Phys., Part 1, vol. 30, p. 3700 (1991)

27. James S. Im, H. J. Kim, and Michael O. Thompson, Appl. Phys. Lett., vol. 63, p.

1969 (1993)

28. James S. Im, H. J. Kim, Appl. Phys. Lett., vol. 64, p. 2303 (1994)

29. S. R. Stiffler, Michael O. Thompson, and P. S. Peercy, Phys. Rev. Lett., vol. 60, p. 2519, (1988).

30. S. D. Brotherton, D. J. McCulloch, J. P. Gowers, J. R. Ayres, and M. J. Trainor, J. Appl. Phys., vol. 82, p. 4086, (1997).

31. G. Ottaviani, D. Sigurd, V. Marrello, J. W. Mayer, and J. O. McCaldin, J. Appl. Phys., vol. 45, p. 1730 (1974)

32. L. Hultman, A. Robertson, H. T. G. Hentzell, and I. Engstrom, J. Appl. Phys. Vol. 62, p. 3647 (1987)

33. S. F. Gong, H. T. G. Hentzell, A. E. Robertsson, L. Hultman, S. E. Hormstrom, and G. Radnoczi, J. Appl. Phys., vol. 62, p. 3726 (1987)

34. G. Radnoczi, A. Robertson, H. T. G. Hentzell, S. F. Gong, and M. A. Hasan, J. Appl. Phys., vol. 69, p. 6394 (1991)

35. E. Nygren, A. P. Pogany, K. T. Short, J. S. Williams, R. G. Elliman, and J. M. Poate, Appl. Phys. Lett., vol. 52, p. 439 (1988)

36. R. J. Nemamichi, c. C. Tsai, M. J. Thompson, and T. W. Sigmon, J. Vac. Sci. Technol., vol. 19, p. 685 (1981)

37. G. Liu and S. J. Fonash, Appl. Phys. Lett., vol. 55, p. 669 (1989)

38. R. J. Nemanichi, R. T. Nemanichi, R. T. Fulks, B. L. Stafford, and H. A. Vanderplas, J. Vac. Sci. Technol., A3, p. 938 (1985)

39. Y. Kawazu, H. Kudo, S. Onari, T. Arai, Jpn. J. Appl. Phys., Part 1, vol. 29, p. 2698 (1990)

40. S. W. Russel, J. Li, and J. W. Mayer, J. Appl. Phys., vol. 70, p. 5153 (1991)

41. K. N. Tu, Appl. Phys. Lett., vol. 27, p. 221 (1975)

42. J. H. Kim, J. Y. Lee, Jpn. J. Appl. Phys., vol. 35, p. 2052 (1996)

43. U. Koster, P. Weiss, J. Non-cryst. Solids, vol. 17, p. 359 (1975)

44. Z. Jin, K. Moulding, H. S. Kwok, and M. Wong, IEEE Trans. Elec. Dev., vol. 84, p. 194 (1998)

45. C. Hayzelden, and J. L. Batstone, J. Appl. Phys. Vol. 73, p. 8279 (1993)

46. T. Ma, M. Wong, J. Appl. Phys. Vol. 91, p. 1236. (2002)

47. J. Gu, S.Y. Chou, N. Yao, H. Zandbergen, J.K. Farrer, Appl. Phys. Lett. Vol. 81, p. 2235 (2002)

48. S.-I. Jun, Y.-H. Yang, J.-B. Lee, D.-K. Choi, Appl. Phys. Lett. Vol. 75, p. 1104. (1999)

49. S.-W. Lee, S.-K. Joo, IEEE Electron Dev. Lett. Vol. 17, p. 160. (1996)

50. Y. Wu, J.G. Duh, J. Mater. Sci. Lett. Vol. 9, p. 583, (1990)

51. F. Secco d'Aragano, J. Electron. Soc. Vol. 119, p. 948. (1972)

52. Z. Jin, K. Moulding, H.S. Kwok, M. Wong, IEEE Trans. Electron. Dev. Vol. 46   p. 78. (1999)

53. J. Jang, S.K. Park, K.H. Kim, B.R. Cho, W.K. Kwak, S.Y. Yoon, J. Appl. Phys. Vol. 88, p. 3099. (2000)

54. D.R. Gaskell, Introduction to the Thermodynamics of Materials, Taylor & Francis, Washington, DC, p. 544. (1995)